iScience

CellPress
OPEN ACCESS

Article

Characterization of cell-to-cell variation in nuclear transport rates and identification of its sources

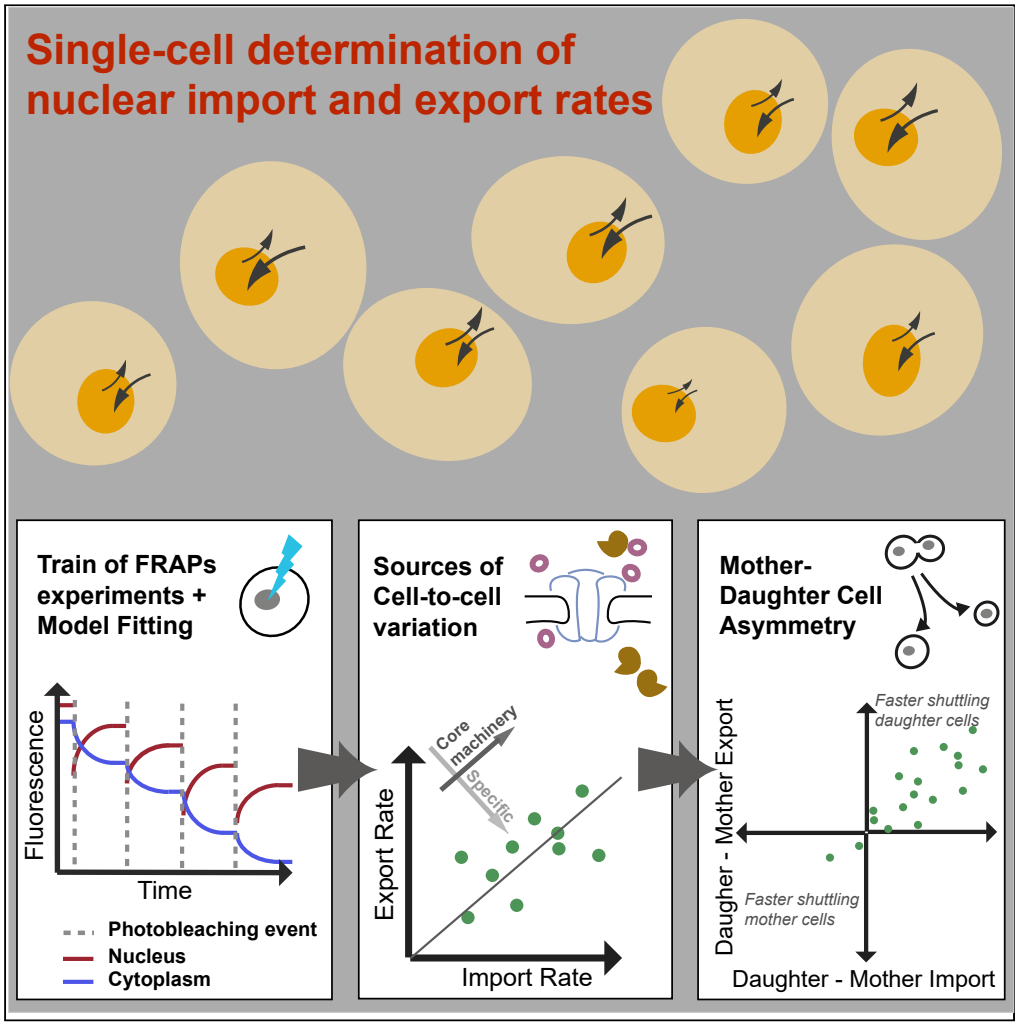

Lucía Durrieu, Alan Bush, Alicia Grande, ..., Andrea Katz, Gunnar Cedersund, Alejandro Colman-Lerner

colman-lerner@fbmc.fcen.uba.ar

Highlights

Sequential FRAPs allow precise estimation of nuclear shuttling rates in single cells

There is high cell-to-cell variation in nuclear import and export rates

Most cell-to-cell variation stems from variability in core transport machinery

Ace2 daughter-cell enrichment is due to higher import rates in that cell type

Durrieu et al., iScience 26, 105906
January 20, 2023
https://doi.org/10.1016/j.isci.2022.105906

iScience

CellPress
OPEN ACCESS

Article

Characterization of cell-to-cell variation in nuclear transport rates and identification of its sources

Lucía Durrieu,[1,2,4] Alan Bush,[1,2,3,4] Alicia Grande,[1,2] Rikard Johansson,[3] David Janzén,[3] Andrea Katz,[1] Gunnar Cedersund,[3] and Alejandro Colman-Lerner[1,2,5,*]

SUMMARY

Nuclear transport is an essential part of eukaryotic cell function. Here, we present scFRAP, a model-assisted fluorescent recovery after photobleaching (FRAP)-based method to determine nuclear import and export rates independently in individual live cells. To overcome the inherent noise of single-cell measurements, we performed sequential FRAPs on the same cell. We found large cell-to-cell variation in transport rates within isogenic yeast populations. For passive transport, the variability in NPC number might explain most of the variability. Using this approach, we studied mother-daughter cell asymmetry in the active nuclear shuttling of the transcription factor Ace2, which is specifically concentrated in daughter cell nuclei in early G1. Rather than reduced export in the daughter cell, as previously hypothesized, we found that this asymmetry is mainly due to an increased import in daughters. These results shed light on cell-to-cell variation in cellular dynamics and its sources.

INTRODUCTION

Isogenic cells, grown under identical conditions, display heterogeneity in their molecular contents. This leads to variation in their physiological states, potentially causing different cellular responses and cell fate choices. Variability emerges partly as a result of the stochastic nature of chemical reactions -specially transcription-,[1–3] but also from fluctuations in other processes, such as the mitotic segregation of materials.[4] In eukaryotes, preexisting differences among cells, such as in protein expression capacity, are the main sources of variation.[3,5–11] These variable non-genetic traits may be passed to their descendants as cells divide, sometimes for several generations, impacting cell function.[7,12–16]

Regulation of nuclear transport influences important cellular processes, including gene expression regulation and signal transduction. Despite its centrality, intrapopulation variability in transport rates has not been studied. Molecules move between the nucleus and the cytosol through 66 MDa nuclear pore complexes (NPCs) embedded in the nuclear envelope, which in *Saccharomyces cerevisiae* consist of 30 different nucleoporins[17] (human NPC are 110 MDa, containing 34 different nucleoporins). Passage may occur in two modes: passive diffusion for small molecules (up to 40 kDa[18] or ~5 nm diameter[19,20]), or facilitated translocation for small and big species.[21] In the latter, translocation is coupled to the transport of the small GTPase Ran, enabling net movement of cargoes against their chemical gradient through the dissipation of the primary gradient of Ran-GTP. Facilitated translocation requires specific interactions between the translocating species and constituents of the NPC and is therefore a highly selective and regulated process. Cell-to-cell variation in nuclear transport rates could thus arise from several sources: variation in passive transport should depend only on the number and quality of nuclear pores, while active transport could be affected additionally by the number of specific transporters, their activation state, the magnitude of the Ran-GTP gradient, and variability in the regulation of the affinity of the cargo for the transporters.

S. cerevisiae cells divide by budding, a polarized process that produces a new cell, the daughter. Transiently, daughters constitute a different cell type, in part as a result of two asymmetric (mother- or daughter-specific) genetic programs. One program drives HO expression in mothers[22–24] while in the other program the transcription factor Ace2 induces in the early G1 of daughter cells the expression of a group of

[1]Department of Physiology, Molecular and Cellular Biology, School of Exact and Natural Sciences, University of Buenos Aires (UBA), C1428EGA, Argentina

[2]Institute of Physiology, Molecular Biology and Neurosciences, National Council of Scientific and Technical Research (IFIBYNE-UBA-CONICET), C1428EGA, Argentina

[3]Department of Biomedical Engineering, Linköping University, Linköping, Sweden

[4]These authors contributed equally

[5]Lead contact

*Correspondence: colman-lerner@fbmc.fcen.uba.ar

https://doi.org/10.1016/j.isci.2022.105906

genes, including chitinase, involved in cell separation.[25] Although the ultimate mechanism that causes Ace2 asymmetric activity is not completely defined, the control of Ace2 localization has been extensively studied. Ace2 subcellular localization is cell-cycle controlled, depending on a layered regulation of its nuclear import and export. Although constantly shuttling in and out of the nucleus,[26] from late G1 until the end of metaphase Ace2 is mostly cytoplasmic.[27,28] Net nuclear entry at the beginning of anaphase[25,28,29] (note that, as in all fungi, mitosis in yeast does not involve nuclear envelope breakdown[30]), is triggered when the phosphatase Cdc14, released from the nucleolus by the mitotic exit network,[31] removes the Cdc28-dependent phosphorylations on Ace2. Cdc14 additionally activates the kinase Cbk1.[32] Active Cbk1 enhances Ace2 nuclear enrichment by phosphorylating it near its nuclear export signal (NES), impairing its interaction with the exportin Crm1.[28,32–36] Even at this pre-cytokinesis stage when the nuclei are still connected, Ace2 appears preferentially enriched in the nascent daughter's nucleus.[25] This asymmetry is perhaps helped by the separation of the mother-daughter nucleoplasms due to the geometric constraints of dividing nuclei.[29] After cytokinesis, Ace2 leaves the mother nucleus but stays in that of the daughter until mid G1.[25,27–29,31,33,37,38] It is in this period in which Ace2 induces its target genes. Thus, the current view is that the asymmetric localization of Ace2 derives from inhibited nuclear export in daughter cells.[39]

Herein, we developed a method to monitor nuclear transport rates in single cells using the optical technique fluorescence recovery after photo bleaching (FRAP),[40,41] which we termed scFRAP. We used this method to obtain both nuclear import and export rates in single live yeast cells. We applied scFRAP to the study of three proteins: as a passively diffusing molecule, we used yellow fluorescent protein (YFP); as actively transported molecules, we used YFP fusions to Ace2 as well as Fus3, a mitogen-activated protein (MAP) kinase in the yeast pheromone response pathway. The obtained measurements were used to determine the degree, sources, and heritability of cell-to-cell variation both in the structural components of the nuclear pore as in their function, reflected in their nuclear transport rates. Additionally, these results provide valuable insights into the mechanism behind Ace2 asymmetric localization.

RESULTS

A train of fluorescent recovery after photobleaching enables robust estimation of nuclear transport rates in single cells

Transport between cellular compartments *in vivo* is frequently studied using FRAP.[42–44] In this technique, a perturbation is introduced by photobleaching a small area of a cell, usually with a laser. Then, this region is monitored as unbleached, bright molecules move into it, resulting in an increase (*recovery*) of the fluorescence signal. While FRAP experiments are performed in single cells, the subsequent analysis is usually done over averages of multiple cells. This is because it is difficult to obtain data from single cells with high signal-to-noise ratio (SNR) without using long exposures and/or more intense illumination, which leads to subsequent photodamage. We reasoned that performing sequential (a "train") of FRAPs on the same cell (Figure 1A) should help improve the single-cell information (without excessive exposure or intensities), potentially avoiding the need for averaging over many cells. We assessed this possibility using a simple mathematical model (Figure 1B) of two compartments and one shuttling species, in a fluorescent or photobleached state. We considered the photobleaching reaction to be irreversible. Fluorescent and photobleached proteins used the same import and export rates, as they are indistinguishable from the transport machinery. We simulated data consisting of trains of 1-5 FRAPs, using a range of realistic kinetic parameters. We introduced different levels of additive white noise to the simulated data, as it is the sort of noise expected from microscopy experiments.[45] Then, to test whether the transport rates could be estimated reliably, we analyzed the simulated data in the same way as the experimental data (described later in discussion). For very high-quality data, such as with an SNR of 50 or more, we recovered the exact rates from single FRAP experiments (mean fitted export rate = 0.92 s^{-1} SD = 0.05, true export rate = 0.90 s^{-1}) (Figure 1C). However, more likely scenarios with lower SNR showed problems. For an SNR of 5, when a single FRAP was performed, the estimated parameters had large dispersion and deviated from the simulated value significantly (mean fitted export rate = 1.57 s^{-1} SD = 2.37, true export rate = 0.90 s^{-1}) (Figure 1C). In this case, increasing the number of FRAPs per train improved the accuracy of the recovered parameters. Notably, trains of only 4 FRAPs resulted in parameter fits consistently close to the true value, even with SNR as low as 5 (mean fitted export rate = 1.05 s^{-1} SD = 0.30, true export rate = 0.90 s^{-1}) (Figure 1C). Interestingly, the biggest improvement was obtained with the addition of the second FRAP on the train (Figure 1C). Altogether, our theoretical analysis showed that performing trains of 4 FRAPs would suffice to determine nuclear import and export rates in single cells, even for noisy single-cell data.

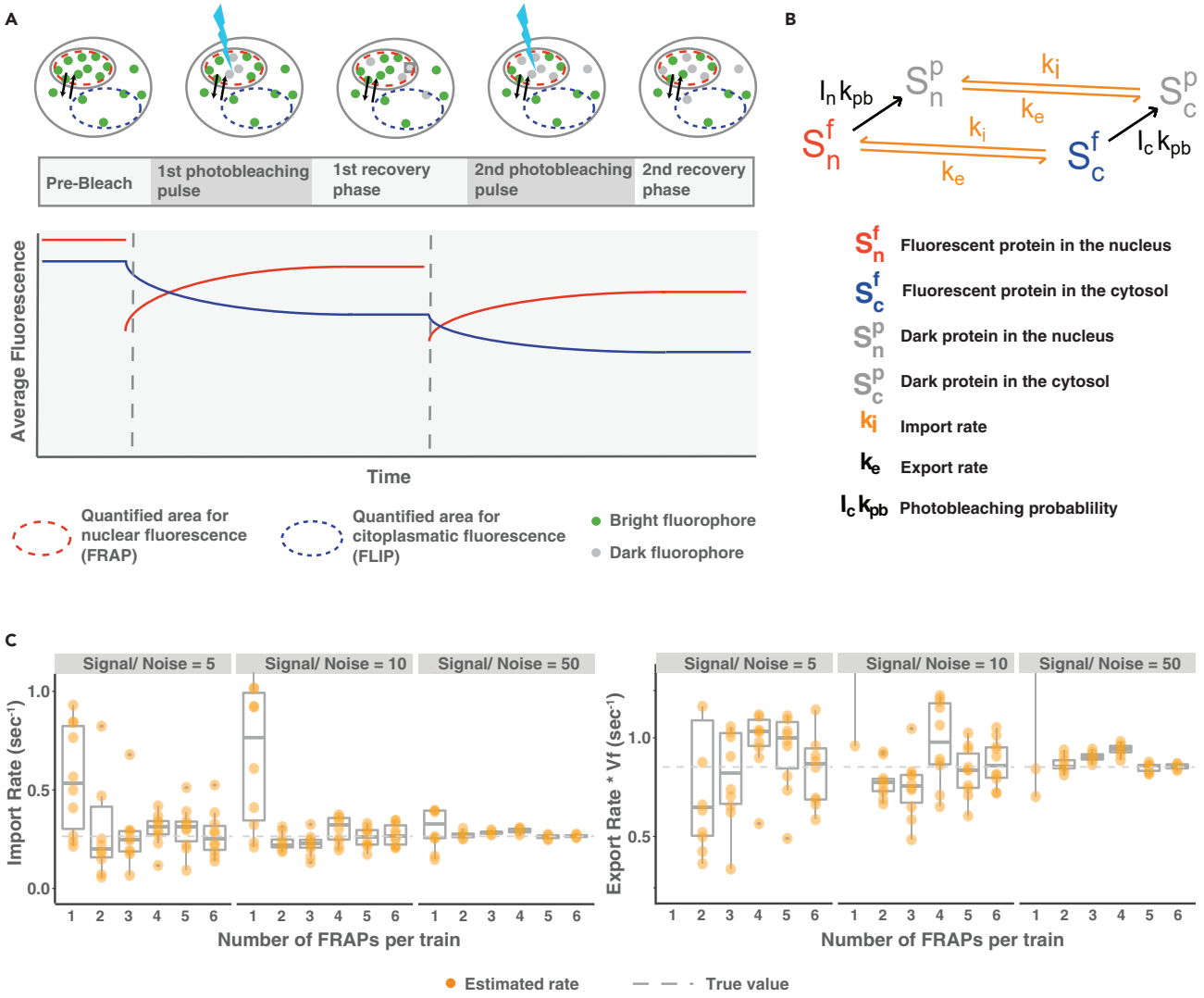

Figure 1. Trains of FRAPs allow the estimation of nuclear import and export rates in single cells even under low signal-to-noise conditions

(A) Schema of an essay with a train of 2 FRAPs.

(B) Reactions schematic in the model used for data simulation and fitting.

(C) Boxplots show import (left) and export (right) obtained by fitting simulated data ($K_I = 0.4\ s^{-1}$, $K_{EV} = 0.9\ s^{-1}$) of trains of different numbers of FRAPs to which noise was added to achieve the signal-to-noise indicated. Data were simulated with $K_I = 0.4\ s^{-1}$, $K_{EV} = 0.9\ s^{-1}$, gray dotted line (the same qualitative results were observed with other parameters). Notice that 4 FRAPs (but not 1), allow consistent recovery simulated parameters, even at realistic noise levels.

Determination of nuclear transport rates in single cells

Based on the above analysis, we developed an experimental protocol and analysis pipeline, which we termed scFRAP (single-cell FRAP), to estimate nuclear export and import rates independently for single cells (see the Data S1) (Figures 2A, S1). Briefly, we performed trains of 4 FRAPs in yeast cells expressing either free YFP or a YFP fusion protein. We fitted the obtained data to an ordinary differential equations model that is an extension of the one described in Figure 1B (Figure 2B), in which we included the possibility that a fraction of the species be "fixed" (not shuttling) in the timescale of the experiment (e.g., molecules bound to the DNA in the nucleus).

In order to minimize potential variation in the transport rates due to the cell cycle, we restricted our measurements to cells at the beginning of G1 by assessing the localization of two proteins: Myo1-mCherry, a component of the actomyosin ring in the bud neck that disappears upon the completion of cytokinesis,[46] and CFP-Ace2, which translocates to the nucleus at the end of mitosis and remains nuclear during early G1.

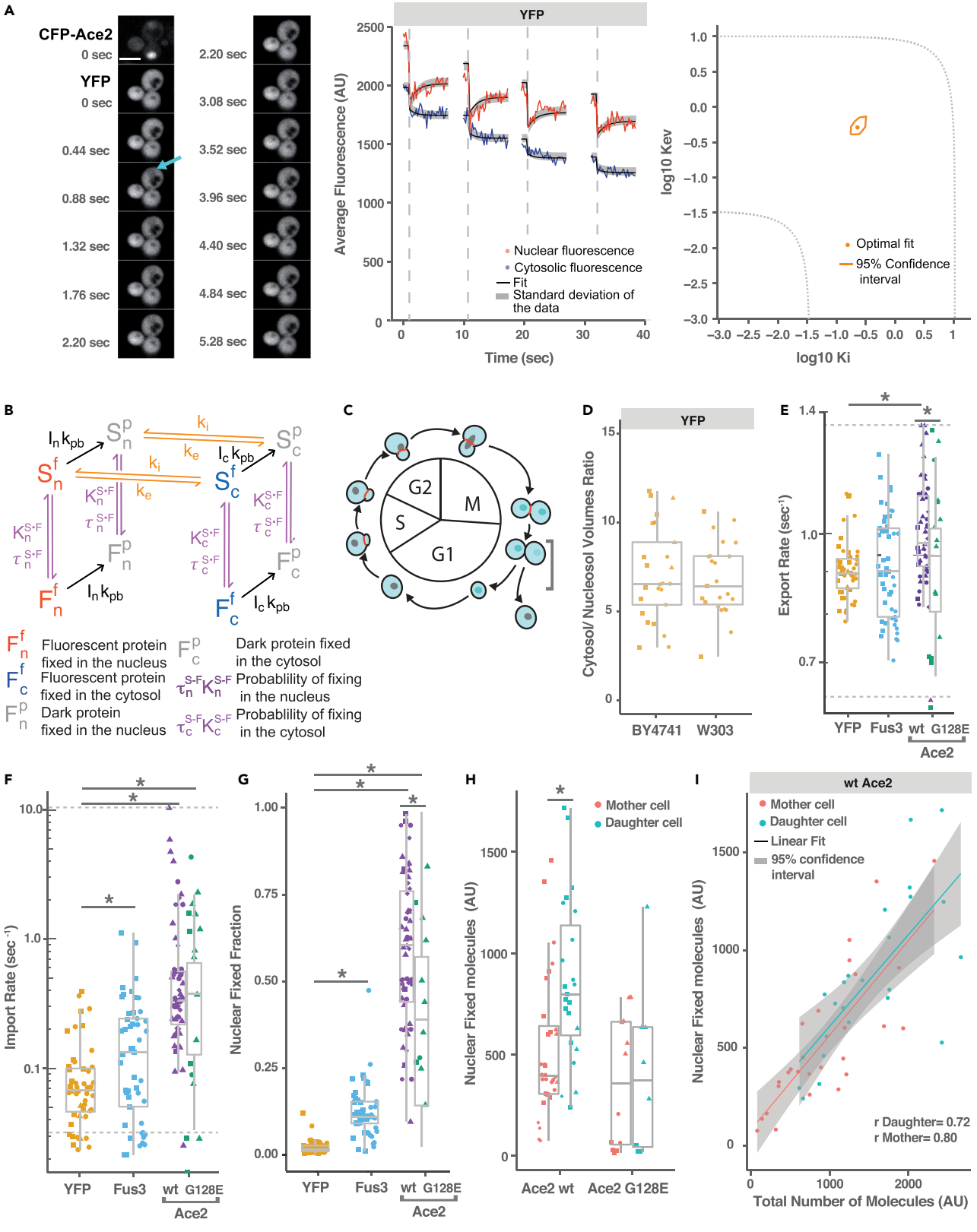
A
CFP-Ace2
0 sec
YFP
0 sec
0.44 sec
0.88 sec
1.32 sec
1.76 sec
2.20 sec
2.20 sec
3.08 sec
3.52 sec
3.96 sec
4.40 sec
4.84 sec
5.28 sec
YFP
Average Fluorescence (AU)
Time (sec)
Nuclear fluorescence
Cytosolic fluorescence
Fit
Standard deviation of the data
log10 Kev
log10 Ki
Optimal fit
95% Confidence interval
B
Fluorescent protein fixed in the nucleus
Fluorescent protein fixed in the cytosol
Dark protein fixed in the nucleus
Dark protein fixed in the cytosol
Probablility of fixing in the nucleus
Probablility of fixing in the cytosol
C
G2
M
S
G1
D
YFP
Cytosol/ Nucleosol Volumes Ratio
BY4741
W303
E
Export Rate (sec-1)
YFP
Fus3
wt
G128E
Ace2
F
Import Rate (sec-1)
G
Nuclear Fixed Fraction
H
Mother cell
Daughter cell
Nuclear Fixed molecules (AU)
Ace2 wt
Ace2 G128E
I
wt Ace2
Mother cell
Daughter cell
Linear Fit
95% confidence interval
r Daughter= 0.72
r Mother= 0.80
Total Number of Molecules (AU)

Figure 2. Experimental determination of nuclear transport rates in single cells

(A) Example of confocal-microscopy images from a representative FRAP experiment. **Left:** Time lapse images of a mother-daughter cell pair expressing Ace2-CFP and free YFP. A single image of Ace2-CFP (top left) was acquired to assess the cell-cycle stage. Then, the FRAP experiment was performed on YFP. Only the first FRAP in a train of four is displayed. After 5 initial pictures, the nucleus was photobleached (cyan arrow), then 30 images were taken to follow the recovery. Pictures were taken every 0.22 s, but only one of the two are shown. Scale bar: 5 mm. **Middle:** Fluorescence intensity curves (red: nucleus, blue: cytoplasm) and fittings (black). The dotted gray lines signal the times of the photobleaching events. **Right:** Likelihood profile analysis (see Methods). Plot shows log 10 K_{EV} vs log10 K_I. The orange dot corresponds to the best fit and the line enclosing it delimits the 95% confidence interval (i.e. all acceptable values). Note that a closed area indicates that both rates can be identified independently. The dotted lines show the boundaries of parameter values that can be estimated using our experimental protocol (limited by the time resolution and duration of the experiment).

(B) Diagram of the reactions included in the full model used for fitting the experimental data. In comparison to the model in 1B, we added fixed molecules (F) in the cytosol (F_c) or nucleus (F_c)was added. These fixed fractions can be photobleached with the same probability than the shuttling fractions.

(C) Diagram of the yeast cell cycle. The localization of the Ace2 protein is depicted in cyan, and the actomyosin ring separating the cells, visualized through Myo1-mCherry, is depicted in red. Yeast in the desired cell cycle state for the experiments was chosen based on the morphological, Ace2-CFP, and Myo1 information, and is marked with a square bracket.

(D) Ratio of cytosol/nucleosol diffusion-available volumes, estimated assuming $K_{EV} = K_I$ for freely diffusible YFP. The points represent individual cells. The measurements were performed in two yeast strains with different backgrounds (S288C, n = 25, and W303, n = 23) and showed no statically significant differences (Mann-Whitney-Wilcoxon test, p value = 0.701).

(E-F) Estimated nuclear transport rates for the proteins YFP (n = 58), Fus3-YFP (n = 48) and Ace2-YFP (n = 49) and Ace2 G128E-YFP (n = 20). The points represent individual cells. Export rates between WT and G128E-mutant Ace2 are significantly different (Mann-Whitney-Wilcoxon test, p value = 0.032, indicated by the asterisk), but import rates are not (Mann-Whitney-Wilcoxon test, p value = 0.795). Distinct symbol shapes indicate experiment replicates.

(G) Fraction of the total amount of proteins that is fixed in the nucleus (not shuttling between nucleus and cytosol). The points represent individual cells. Mann-Whitney-Wilcoxon test indicates that the G128E mutant has smaller values than wt Ace2 (p value = 0.003), marked with an asterisk. Distinct symbol shapes indicate experiment replicates.

(H) Number of nuclear fixed Ace2 molecules in mother and daughter cells, for WT and G128E mutant strains. The points represent individual cells. For Ace2 WT, daughter cells have more fixed molecules than mothers (Mann-Whitney-Wilcoxon test, p value = 0.001). The asterisk indicates statistical significance ($p < 0.05$). In the G128E mutant no differences were observed (Mann-Whitney-Wilcoxon test, p value = 0.604). Distinct symbol shapes indicate experiment replicates.

(I) Plot shows fixed vs total Ace2. r is the correlation coefficient. The points represent individual cells. Slope and intercept are not statistically different between daughters and mothers. In all panels with boxplots the lower and upper hinges correspond to the first and third quartiles (the 25th and 75th percentiles), the line in the box marks the median of the distribution, the upper whisker extends from the hinge to the largest value no further than 1.5 * IQR from the hinge (where IQR is the inter-quartile range, or distance between the first and third quartiles). The lower whisker extends from the hinge to the smallest value at most 1.5 * IQR of the hinge.

As explained above, Ace2 remains nuclear for a longer period in daughter cells than in mothers[25] (Figure 2C). Thus, we used cells that did not have Myo1-mCherry at the bud-neck while at the same time having nuclear CFP-Ace2 in both mothers and daughters (Figure 2C, gray bracket). Choosing this moment in the cell cycle enabled us to measure the nuclear transport of Ace2 in mothers and daughters, in order to shed light on the nature of its asymmetric behavior.

Fitting of the FRAP data yielded parameters K_I and K_{EV}. The first represents the import rate, while the latter corresponds to the export rate multiplied by **V**, the ratio of the diffusion-accessible volumes of the cytoplasm and the nucleus. Thus, to determine transport rates, we needed to determine **V**. The value of **V** is of interest by itself, and it should not be confused with the ratio of the cytoplasm to the nucleus geometric volume, since not all of the cytoplasmic and nuclear volumes are available for diffusion, due to the presence of organelles, macromolecules, chromatin and other cellular materials precluding diffusion of the protein of interest. We reasoned that **V** for each cell can be obtained for a molecule with identical import and export rates, such as YFP, which is small enough to diffuse passively through the nuclear pores, and it does not interact with any importin or exportin. Therefore, we first measured transport of YFP. To do that, we used a haploid BY4741 yeast strain (S288C genetic background) expressing YFP controlled by the *ACT1* promoter (P_{ACT1}). After the estimation of the nuclear transport parameters K_{EV} and K_I we calculated the K_{EV} to K_I ratio and obtained a **V** of 7.14 $\pm$ 0.53 (mean $\pm$ SEM) with an SD of 2.64 (Figure 2D). We performed the same measurement in another commonly used genetic background, W303, and obtained similar values **V** of 6.84 $\pm$ 0.43 with an SD of 2.08 (Figure 2D). This yielded import and export rates for YFP with a median value of 0.06 $\pm$ 0.02 s^{-1} with and SD of 0.073 s^{-1} (Figures 2E-2F, Table 1). To estimate rates for other proteins, we used the average value of **V** calculated from the YFP measurements. Doing so introduced a small uncertainty in the determination of the export rate.

We then applied scFRAP to study the nuclear transport of Ace2 using a strain expressing P_{ACE2}-*YFP-ACE2*. For comparison, we additionally measured in a strain expressing P_{FUS3}-*FUS3-YFP*, coding for an unrelated protein kinase Fus3, central in the pheromone response pathway, which also shuttles between the nucleus

Table 1. Estimated parameters from the scFRAP experiments

Protein	Export Rate (median ± se) [sec-1]	CV Export Rate	Import Rate (median ± se) [sec-1]	CV Import Rate	Tau (median ± se) [sec]	CV Tau	Nuclear Fixed Fraction (median ± se) [sec-1]	CV Nuclear Fixed Fraction
YFP (BY4741)	0.06 ± 0.01	0.87	0.07 ± 0.01	0.89	2.10 ± 0.25	0.54	0.01 ± 0.01	1.25
YFP (W303)	0.06 ± 0.02	0.86	0.07 ± 0.02	0.89	2.02 ± 0.21	0.51	0.01 ± 0.00	0.59 s
Fus3 (W303)	0.06 ± 0.02	1.16 b	0.13 ± 0.03 e	1.12 h	1.72 ± 0.36	0.94 m	0.11 ± 0.01 p	0.64 t
Ace2 (BY4741)	0.11 ± 0.04 a	1.30 c	0.33 ± 0.24 f	1.85 i	0.93 ± 0.35 k	2.07 n	0.61 ± 0.03 q	0.37 u
Ace2 G128E (BY4741)	0.08 ± 0.04 ρ	1.26 d	0.37 ± 0.11 g	1.06 j	0.88 ± 0.42 l	0.99 o	0.39 ± 0.06 r, φ	0.70 v

To assess the statistical significance of the estimated parameters Export rate (K_{EV}), Import Rate (K_I), tau, and nuclear fixed fraction, a Welch two-sample t-test was performed on the log-transformed values. All proteins were compared to YFP (BY4741), but only significant scores are indicated (Latin letters). a: p = 5.8 e−4, e: p = 1.8 e−2, f: p = 7.5 e−11, g: p = 4.2 e−06, k: p = 1.7 e−07, l: p = 4.3 e−2, p: p = 1.1 e−11, q: p < 2.2e-16, r: p = 8.6 e−06. Ace2 G128E mutant was additionally compared with Ace2 WT, and significant differences are indicated with Greek letters. ρ: p = 4.4 e−2, φ: p = 8.0 e−3. The statistical significance of the differences in cell-to-cell variation was evaluated by an F-test to compare the variances of the log-transformed values. b: p = 4.5 e−3, c: p = 3.8 e−3, d: p = 1.6 e−3, h: p = 3.2 e−2, i: p = 1.0 e−2, j: p = 2.4 e−2, m: p = 5.1 e−3, n: p = 4.9 e−3, o: p = 8.5 e−3, s: p = 1.3 e−05, t: p = 3.4e-07, u: P = < 2.2e-16, v: P =< 2.2e-16.

and the cytoplasm.[47] When fused to YFP, these proteins have a size of ~115 kDa and ~69 kDa, respectively. The former is too large to shuttle by passive diffusion through the NPCs, while the latter is too close to the size limit to be certain.[18] In fact, a previous FRAP-based study showed that a Fus3-GFP fusion shuttles both by facilitated transport and to a lesser extent by passive diffusion.[48]

The export rate for Fus3-YFP did not differ from that of YFP, but Fus3 import was faster (Figures 2E-2F, Table 1). The fact that we were able to fit well Fus3 data with our model with a single export and a single import rate, shows that the kinetics from the active and passive transport are in the same order and thus our estimate reflects an aggregate of the two, an effective transport rate.

In contrast, import and export of YFP-Ace2 were faster than YFP rates (Figures 2E-2F, Table 1). We also measured the behavior of the mutant Ace2-G128E,[49] which shows an altered cellular localization, persisting in the mother cell nucleus to mid-G1 phase, similar to daughter cells.[25,35] This mutation lies within a NES region,[50] and has been shown to block the interaction of Ace2 with the exportin Crm1 by yeast two-hybrid.[35] Moreover, a peptide with a similarly behaved mutation, F127V, showed no detectable interaction with Crm1.[28] In agreement with these results, our scFRAP revealed that export of Ace2-G128E was reduced (Mann-Whitney-Wilcoxon test, p value = 0.03), while its import rate was unchanged (Figures 2E-2F, Table 1). However, significant export remained, suggesting that the interaction with Crm1 is not completely lost in the mutant, perhaps hinting at the existence of another Crm1-interacting region (see Discussion). To rule out export by another exportin, we performed FRAPs of YFP-Ace2 inhibiting Crm1 with leptomycin B. In this condition, there was no detectable fluorescence recovery, indicating that Crm1 is the only relevant exportin of Ace2 (Figure S2). Taken together, these results support the notion that our method is suitable for estimating import and export rates of endogenous proteins in single yeast cells with enough precision to detect functional differences.

Estimation of the amount of non-shutting molecules in the nucleus

The FRAP-analysis method also renders an estimation of the number of non-shuttling ("fixed") molecules present during the experiment in either compartment (Figure 2B). Note that these molecules are only "fixed" in the timescale of the experiment (seconds), but they could be binding and unbinding from their "traps" in a slower timescale. Our analysis suggested that for the proteins studied here there were no fixed molecules in the cytoplasm (see Data S1 Section 3). We found no fixed molecules in the nucleus for the case of YFP (Figure 2G), as expected. In contrast, of the nuclear pool, on average, about 10% of Fus3-YFP and 60% of YFP-Ace2 molecules were fixed (Figure 2G). The MAPK Fus3 targets several DNA-associated substrates in the nucleus, such as the transcription factor Ste12 and its regulators Dig1 and Dig2.[47] Thus, this 10% of fixed molecules could represent Fus3 bound to these species, which themselves do not shuttle.[48] In the case of Ace2, since it is a transcription factor, the high amount of fixed Ace2 molecules likely corresponded to DNA-bound Ace2. Notably, daughter cells had more fixed Ace2 than mothers (Figure 2H), consistent with Ace2 preferential induction of genes in daughter cells.[25] Single-cell analysis revealed

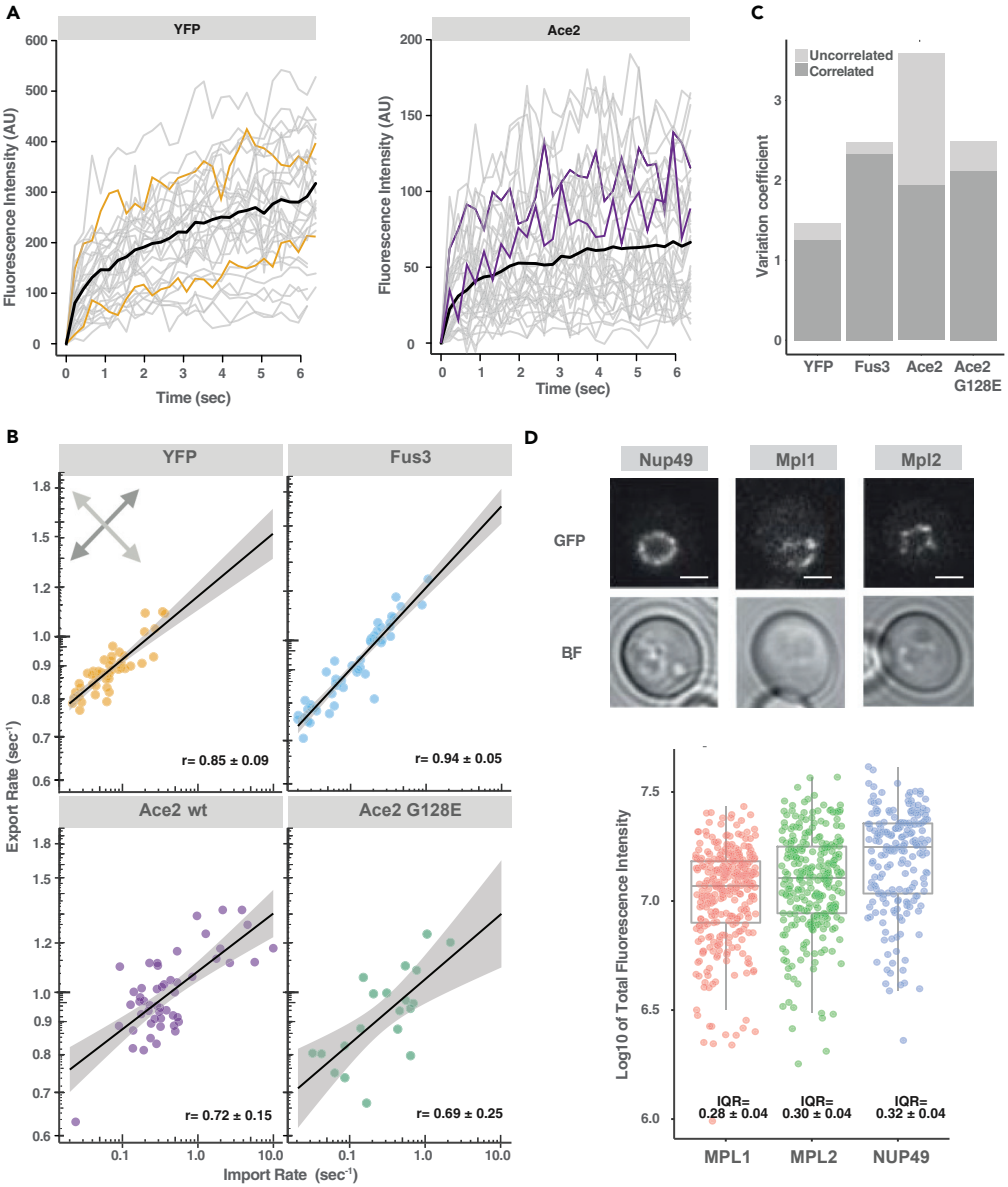

Figure 3. The high cell-to-cell variation in nuclear transport rates is mostly due to the variation of general transport machinery

(A) Individual traces of FRAP experiments in single cells (gray lines). Each line corresponds to the average of the four FRAPs in the train where the first value after photobleaching has been subtracted. The average of all traces is shown in black. Representative fast and slow traces are highlighted in color for both proteins.

(B) Plots show export vs import for the proteins YFP (n = 58), Fus3-YFP (n = 48) and Ace2-YFP (n = 49) and Ace2 G128E-YFP (n = 20). Both axes are on the logarithmic scale. The black line corresponds to the linear model, and the gray shadowed area represents de 95% confidence interval. r values correspond to the correlation coefficient. Errors were calculated by bootstrapping and correspond to a 95% confidence interval. Gray arrows in the left top indicate the direction of the correlation (dark gray) and the anti-correlation (light gray).

(C) Plot shows a quantification of the correlated and un-correlated variation between import and export rates. The correlated components represent the spread of the normalized data in the direction parallel to the linear fit (dark gray arrow on B). The un-correlated component is a measure of the normalized rates perpendicular to the linear fit (light gray arrow in B). The details of the estimators can be found in the STAR Methods section. Correlated variation could be attributed to heterogeneities in general transport machinery, such as NPCs.

(D) Boxplots that show the distribution of frequency of the intensity of the GFP-tagged nuclear pore protein (top). The logarithmic transformation of the data is used. The errors in the IQR were calculated by bootstrapping and correspond to

Figure 3. *Continued*
a 95% confidence interval. **Top:** Representative confocal images of the analyzed nuclear pore proteins. Scale bar: 2 μm. **Bottom:** Total fluorescence of GFP fusions to the indicated nuclear envelope proteins per cell, as quantified from fluorescence intensity (AU). MPL1 (NPC associated, n = 2254), MPL2 (NPC associated, n = 1967) and NUP49 (NPC integral, n = 1442).

that the number of fixed Ace2 molecules in nuclei correlated well with the total number of Ace2 molecules in a cell, independently of cell-type (Figures 2I, S3). This suggested that there was not a particular enhancement of Ace2 DNA binding in daughters, there was just more Ace2 in them. Also, this large correlation means that most of the variation in the nuclear fixed fraction of Ace2 (Figure 2G) can be explained by variation in the total amount of Ace2. In the Ace2-G128E mutant, which exhibits symmetric localization and expression of its target genes,[25] mother cells had a similar number of nuclear fixed YFP-Ace2 molecules than daughters (Figures 2H, S3). Finally, the number of nuclear fixed molecules did not correlate with the import/export rates ratio (Figure S3).

Most of the variability in passive nuclear transport rates stems from variations in the core nuclear transport machinery

Interestingly, we found large cell-to-cell variations in the import and export rates of all three proteins studied (Figures 2E-2F, Table 1). This variability was significantly higher for YFP-Ace2 and Fus3-YFP than for YFP. The high cell-to-cell variation was evident in the raw traces, and thus we do not believe it might be the result of misfitting (Figure 3A).

We then wondered what the sources of the measured variability in rates were. We reasoned that some of it might be due to cell-to-cell differences in the abundance or the activity of components of the core nuclear transport machinery (i.e., those that affect equally import and export, such as NPCs). Variation in the rates of actively transported proteins, however, could additionally be affected by cell-to-cell variability in the abundance of nuclear transporters, regulators, and the Ran-GTP gradient. Importantly, variability in core nuclear transport machinery and the Ran-GTP gradient would impact import and export rates in the same manner, increasing their correlation, while variability in the regulators could affect these rates to different extents, decreasing their correlation.

Thus, to dissect these two sources of variation, we quantified the correlated and un-correlated components of the variability in the rates of each protein[51] (Figure 3C). For the three proteins studied, we found that import and export rates were highly correlated (Figures 3B and 3C). In the case of YFP, this correlated component represented almost all the variation. This result was expected, since YFP passage through the NPC does not require binding to any factors, and thus cell-to-cell variation is most likely dominated by differences in the number or quality of NPCs (see later in discussion). Although more variable than YFP, Fus3 maintained the high import to export rates correlation, indicating that whatever additional factors contribute to the variation, they affect nuclear passage in both directions. Considering that Fus3 transport is at least partially active, we speculated that a relevant factor is the variability in the strength of the Ran-GTP gradient. In contrast, for Ace2, we found a greater amount of un-correlated variability (Figures 3B and 3C), probably because its import and export are individually regulated. Remarkably, Ace2 un-correlated variability was greatly reduced in the mutant Ace2-G128E (Figure 3C). Since the G128E mutation reduces Ace2 interaction with exportin Crm1 and reduces the effective export rate (Figure 2E), the high Ace2 un-correlated variation could be attributed to cell-to-cell variability in the export rate. Heterogeneity in Ace2 export could originate in part in mother-daughter differences, but also in the strong cell cycle regulation of its nuclear localization. Even though we only imaged cells that were traversing a specific, and short, part of the cell cycle (just post cytokinesis) small differences in their actual cell cycle position were unavoidable, which might contribute to variability in the measured transport rates.

To assess whether the co-variation of import and export rates could be due to differences among cells in the number of NPCs, we analyzed, as a proxy, the cell-to-cell variability in the amounts of nuclear pore proteins.[52] We quantified nuclear envelope fluorescence in confocal images of yeast cells expressing three different GFP-tagged proteins: NPC-associated proteins Mlp1 and Mlp2, and the central core component of the NPC Nup49[53] (see Methods) (Figure 3D, top). Interestingly, the magnitude of the cell-to-cell variation in these nuclear pore proteins was similar to that of nuclear transport rates (Compare Figure 3D and YFP values in Figures 2E and 2F). Note that, despite the fact that the nuclear pores fluorescence and the kinetic transport rates are very different quantities with different units, when the logarithm of the measurements is

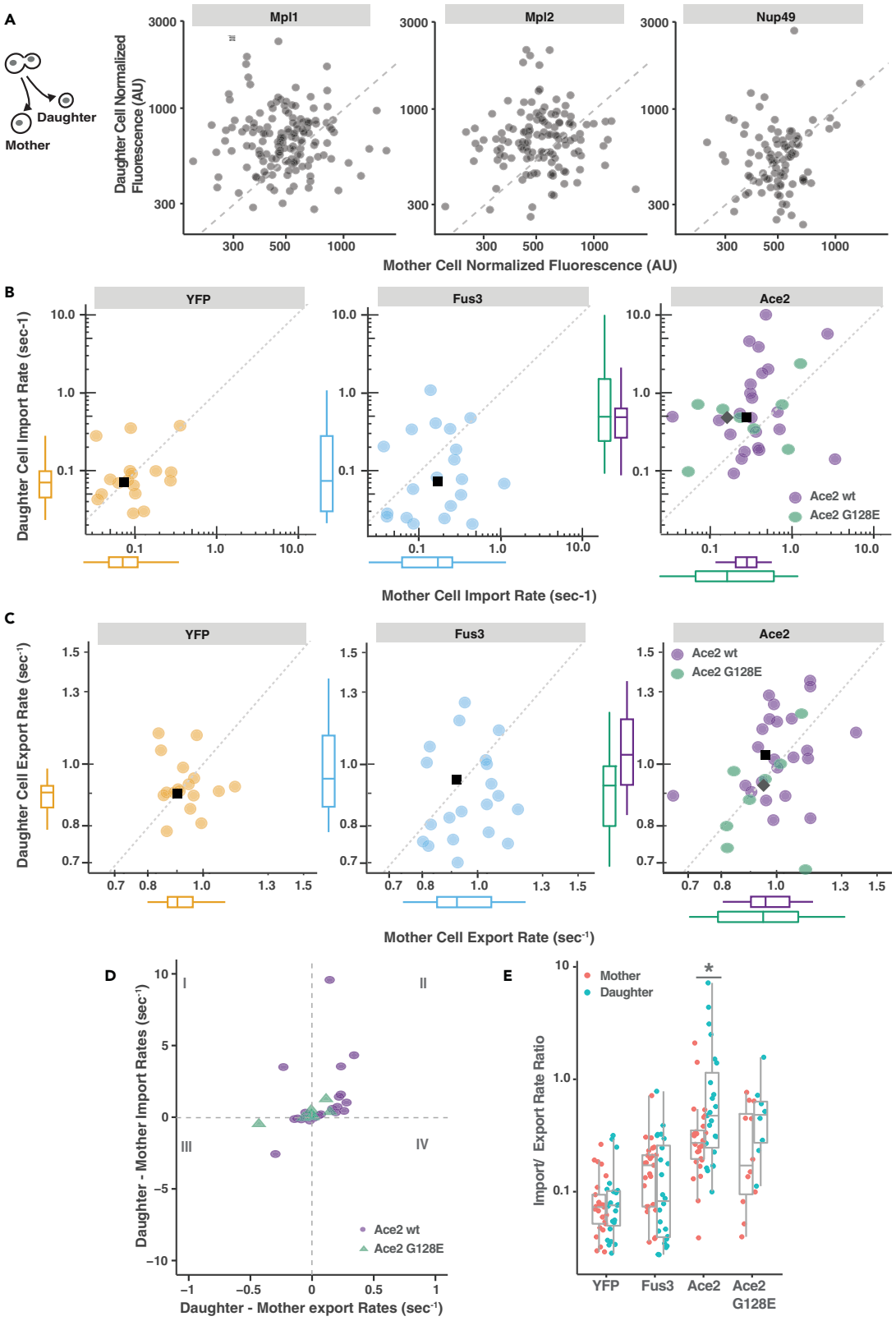
A
Daughter
Mother
Mpl1
Mpl2
Nup49
Daughter Cell Normalized Fluorescence (AU)
Mother Cell Normalized Fluorescence (AU)
B
YFP
Fus3
Ace2
Daughter Cell Import Rate (sec-1)
Mother Cell Import Rate (sec-1)
Ace2 wt
Ace2 G128E
C
YFP
Fus3
Ace2
Daughter Cell Export Rate (sec-1)
Mother Cell Export Rate (sec-1)
Ace2 wt
Ace2 G128E
D
I
II
III
IV
Daughter - Mother Import Rates (sec-1)
Daughter - Mother export Rates (sec-1)
Ace2 wt
Ace2 G128E
E
Mother
Daughter
*
Import/ Export Rate Ratio
YFP
Fus3
Ace2
Ace2 G128E

Figure 4. Mother-daughter cell segregation of NPCs and transport rates

(A) Plots show daughter vs mother normalized nuclear fluorescence (total GFP fluorescence in the nucleus divided by the cell volume) of three NPC components, Mlp1 (left), Mlp2 (middle), and Nup49 (right).

(B-C) Plots show daughter vs mother import rate (B), or export rate (C), obtained for YPF (left, N = 23), Fus3-YFP (middle, N = 24), and YFP-Ace2 (right, WT: green, N-23, or the G128E mutant: purple, N = 8). Boxplots on each axis show the distribution of the variable in that axis. The lower and upper hinges correspond to the first and third quartiles (the 25^{th} and 75^{th} percentiles), the line in the box marks the median of the distribution, the upper whisker extends from the hinge to the largest value no further than 1.5 * IQR from the hinge (where IQR is the inter-quartile range or distance between the first and third quartiles). The lower whisker extends from the hinge to the smallest value at most 1.5 * IQR of the hinge.

(D) Plot of the difference in rates (daughter minus its mother), import vs export for YFP-Ace2 (WT, blue circles), and the G128E mutant (green triangles). Most WT YFP-Ace2 WT cell pairs fall in quadrant II, indicating that the daughter cell has both higher import and export rates, while for the YFP-Ace2-G128E mutant most pairs are close to the origin, indicating small differences.

(E) Ratio of import to export rate for the indicated strains in mothers (red) and daughters (green). A-C, black squares (and gray diamond in C) correspond to the location of the mean of the Y and X axes. The asterisk indicates a significant difference ($p < 0.05$).

taken, the spread of the distributions becomes directly comparable.[54] Taking the inter-quartile range as a measure of spread, we found it to be 0.28 ± 0.04 for Mpl1, 0.30 ± 0.04 for the amount of Mpl2, 0.32 ± 0.04 for Nup49, 0.33 ± 0.07 for the export rate of YFP and 0.38 ± 0.13 for the import rate of YFP. This suggested that the variability in YFP nuclear transport rates might be directly attributable to variability in NPC number. Future work would be needed to measure NPC abundance and transport rates in the same cells to confirm this hypothesis. However, if correct, our results suggest that other possible sources of variation, such as variable amounts of regulators or the quality of the nuclear pores being heterogeneous, have a relatively small contribution to overall variation in transport rates.

Segregation of nuclear pore complexes and nuclear transport rates during cell division are highly noisy

A possible mechanism creating population variability in NPC abundance, which in turn might translate into variation in transport rates, is their random segregation during cell division. To explore this effect, we asked if the amount of NPC proteins was correlated between mother cells and their daughters. (Note that since our measurements were performed just after cell division, it was warranted to assume that there was no substantial contribution of newly synthesized NPC components.) A correlation would indicate that daughters always receive a similar fraction of the NPCs with low segregation noise. Comparison of mother vs daughter NPC numbers revealed no significant correlation (Figure 4A), suggesting that segregation for NPCs is highly noisy. Similarly, nuclear transport rates of YFP did not correlate between mother and daughter cells, nor did those for the actively transported proteins Fus3-YFP and YFP-Ace2 (Figures 4B and 4C). We confirmed all the above results using a similarity measure (Figure S4). These findings show that, even in the first generation, there is no epigenetic inheritance of NPC abundance or nuclear transport rates.

Mother-daughter asymmetry in nuclear transport rates

Another mechanism that could cause population variability would be a systematic asymmetry in the segregation of components during division. As mentioned above, yeast division is polarized, with the mother cell forming the bud that will become a daughter cell. Thus, for example, it could be that daughters receive, on average, more (or less) NPCs, or that they are of a different quality. We found no significant differences between the mother and daughter cell population in nuclear transport rates for either YFP (Mann-Whitney-Wilcoxon test, KE $p = 0.258$, KI $p = 0.306$) or Fus3-YFP (Mann-Whitney-Wilcoxon test, KE $p = 0.689$, KI $p = 0.762$) (Figures 4B-4C, left), indicating that whatever differences might exist between mothers and daughters, these are not sufficiently strong to overcome the noisy segregation of NPCs. Thus, we concluded that NPC function is, in this regard, symmetric (similar in mothers and daughters).

In stark contrast with YFP and Fus3-YFP, for YFP-Ace2 the rates of both import and export were faster in daughter cells than in mothers (Mann-Whitney-Wilcoxon test, KE $p = 0.067$, KI $p = 0.002$) (Figures 4B-4C, right). This difference is reduced in the Ace2 G128E mutant (Mann-Whitney-Wilcoxon test, KE $p = 0.371$, KI $p = 0.039$). In consonance with the above population-level results, we found that, when compared pairwise, most daughter cells have both faster export and import of Ace2 than their mothers (Figure 4D, Mann-Whitney-Wilcoxon test, $p = 0.002$), an intriguing result that would require future studies. It is noteworthy that also the ratio of import to export rate was larger in daughters (Figure 4E). Taken together, these results indicated that the mobile (i.e., not fixed) molecules of YFP-Ace2 shuttle faster and are more nuclear in daughter cells. Finally, this kinetic difference between mothers and their daughters was not observed

for the symmetrically localized YFP-Ace2 G128E mutant (Figures 4D and 4E), free YFP, or Fus3-YFP (SM Figure 4B), so it appears to be related to the specific mechanisms that cause Ace2 asymmetric localization to the daughter cell.

DISCUSSION

Quantitative measurements of dynamic processes in single cells are essential for a system-level understanding of cellular function. Here, we introduced scFRAP, a method that combines an FRAP protocol with an analysis pipeline for the determination of nuclear import and export kinetic rates in intact single cells, suitable for the usually noisy experimental conditions. Additionally, it extracts the fraction of non-shuttling molecules, a parameter of significant biological value. This method, developed for nuclear transport in yeast, may be adapted for other cellular compartments, including membrane-less organelles, as well as for other cell types, such as mammalian cells. We estimated the nuclear transport rates in single cells with two central goals: to obtain a better understanding of cell-to-cell variability in kinetic rates and to study the mechanisms behind a cell-fate decision (the asymmetry in the transcription factor Ace2 that drives a daughter-cell specific genetic program). Our estimations matched well with previous population measurements and were affected as expected by genetic manipulations.

We estimated nuclear transport rates in the order of 0.1 s^{-1}. This number means that, if there are 1000 molecules of a protein X in a yeast cytosol (approximately 1 μM), and 86 nuclear pore complexes in the nuclear envelope,[55] 1.2 molecules of X are imported to the nucleus per second per pore. Our results are entirely compatible with the estimations of 3.3 molecules of GFP exported per pore per second for a 1 μM gradient across the nuclear envelope in isolated oocytes nuclei,[56] the 0.18 NLS-GFP molecules imported NPC^{-1} sec^{-1} in yeast nuclei,[57] the approximately 1 NPC^{-1} sec^{-1} for GGNLS[58] in HeLa cells, and the 2 for GFP NPC^{-1} sec^{-1} for a 1 μM gradient also in HeLa cells.[59] This agreement is remarkable, as the cited studies were performed in a different cell type, with different cargos, and under different conditions. If this similarity is not due to chance, it would imply that NPC permeability has been strongly conserved, at least between fungi and mammals.

Translocation of the actively transported proteins we tested was faster than the passively diffusing YFP. Active transport rates can exceed passive diffusion, sometimes by a large factor, as established by single transporter recordings[56,60] as well as by bulk import measurements in permeabilized cells.[61,62] The pheromone response pathway MAPK Fus3 was exported at rates similar to YFP, but it was imported twice as fast. From this, we concluded that at least a sizable fraction of Fus3-YFP is actively transported. This is in good agreement with earlier findings[48] that showed that blocking active transport reduced, but did not eliminate, Fus3 nuclear transport.

We found large cell-to-cell variation in transport rates for the three proteins studied. When we compared import and export rates in single cells, we found that most of this variation was correlated, with some cells having fast and some cells slow shuttling dynamics. Considering that YFP only crosses the NPC by passive diffusion, this finding suggested that the heterogeneity in the transport rates comes from variability in core nuclear transport machinery. A possible source of such variation could be variability in NPC abundance, the extent of which we measured by direct labeling of NPC components. Thus, heterogeneity in the number of NPCs could be the main determinant of variability in the kinetic rates.

The actively transported proteins Fus3 and Ace2 had higher levels of correlated variation than YFP. The molecular mechanism responsible could be intrinsic to Fus3 or Ace2 transport, or it might be extrinsic and as such be a more general phenomenon, impacting all actively transported proteins. A general effect could result, for example, from variability in the strength of the Ran-GTP gradient. We found no previous data investigating this possibility.

Variability in the core transport machinery (leading to the correlated variability import and export rates we showed here) would only affect the shuttling speed of mobile proteins, without affecting their net subcellular localization (which is dictated by the ratio of import to export). Whether and how shuttling speed could control protein activity has not been established. One possible scenario could arise for a protein whose nuclear transport is coupled to its post-translational modification in only one compartment and the removal of that modification in the other. If this modification proceeds at a rate slower than transport, then proteins that shuttle faster would be less available for the modifying enzyme.

Naturally, variability in net import or export would be important for molecules that are transported in only one direction, such as newly synthesized RNA molecules. Cells with faster nuclear export should have mRNAs more readily available for translation, leading to a faster expression response. In the case of Fus3, one could imagine that cells with faster Fus3 shuttling might be able to mount a transcriptional response to mating pheromone faster, which might lead to faster mating. Thus, it would be interesting to further study the basis of this regulation and to determine if MAPKs in other systems, such as mammalian cells, also have variable shuttling speed.

According to our estimations, the effective volume in the yeast cytosol available for diffusion is 7 times larger than that volume in the nucleosol. Since the yeast nucleus is approximately 14 times smaller than the cell, as determined using geometrical considerations only,[63] consequently the cytoplasm is twice as occupied as the nucleus, perhaps due to the presence of organelles. Indeed, from published data obtained by soft X-ray microscopy,[64] we estimated a ratio of 8 subtracting from the cytoplasm volume that of the vacuole, mitochondria, and lipid bodies. Also, our number agrees well with electron microscopy-based estimations of the cell/nucleus (subtracting organelles) volume of 6.25.[65] The agreement is remarkable since we obtained this ratio solely from the dynamics of YFP in the FRAP experiments.

Cellular division involves the segregation of all its components between descendant cells. While a noisy partitioning of cellular components would increase the population variability,[4] its counter-side, "cellular heritability," would limit it.[66] Interestingly, our results show no heritability in either the number of NPCs or nuclear transport rates, suggesting that partitioning of the nuclear transport machinery during cell division is highly stochastic. Epigenetic heritability of cellular characteristics has been reported in several processes, where it was found to last between 2 and 10 generations, with first-generation correlations of 0.6-0.9.[7,14,16,66,67] There are also reports of noisier processes where no heritability was found.[15,68]

Although the ultimate mechanism that causes Ace2 asymmetric localization to the daughter cell nucleus is still unknown, our FRAP measurements provide notable insights. First, consistent with reports of enhanced transcription in daughter cells, we found a higher amount of Ace2 fixed in the nucleus in this cell type, which seems to be a consequence of the higher concentration of Ace2 in the nucleus of daughters, not the result of additional regulation. Second, our results do not entirely match the current view of Ace2 localization based on the phosphorylation of the NLS and NES. According to this model, Ace2 is constantly shuttling in and out of the nucleus[27,28,50] with the balance biased toward the cytoplasm until the end of metaphase due to Cdc28-dependent phosphorylation near its C-terminal NLS.[31] In anaphase, the drop in Cdc28 activity stops the phosphorylation of these sites and the activation of the phosphatase Cdc14 causes their removal. This uncovers Ace2 C-terminal NLS, shifting the balance in favor of nuclear accumulation, both in mothers and in daughters. According to the current view, the higher concentration of Ace2 in daughters results from reduced export in these cells relative to their mothers. This idea originated in the observation that Cbk1 phosphorylates Ace2 in its NES and that phosphorylated peptides of that region result in no detectable interaction with the exportin Crm1, similar to the effect of the G128E and F127V mutations.[28] Thus, if Cbk1 phosphorylates Ace2 preferentially in daughter cells, reduced export in this cell type could be the reason of the observed enrichment of Ace2 in daughters' nuclei. However, to our surprise, we found the opposite, namely, export (and import) was faster in most daughters than in their mothers. Thus, we obtained no direct evidence of reduced export in daughter cells expressing wild-type Ace2. In addition, when we measured the Ace2 NES mutant G128E, which has greatly reduced interaction with Crm1,[35] we found only a modest (albeit significant) reduction in the export rate. This suggests that Ace2 might indeed contain a second Crm1 interacting region, as previous results hinted at,[26] given that we ruled out the significant export activity by a Crm1-independent mechanism. Thus, according to our data, the higher ratio of import to export rate necessary to concentrate Ace2 in daughters' nuclei seems to require enhanced import to offset the high export in daughters. We note that our results are biased to the early stages of the establishment of asymmetric localization, a time window in which it is still possible to detect Ace2 in mother nuclei. It is conceivable that at a later stage, transport dynamics of Ace2 change so that export does diminish in daughters and speeds up in mothers.

Altogether, this study shed light on cell-to-cell variation in the kinetic rates of nuclear transport and its sources. It is likely that a similar heterogeneity occurs in other cellular processes. High population variability in kinetic rates could have a big impact on cellular function, and future studies will be needed to understand how it propagates and the consequences it has.

Limitations of the study

The imaging protocol for the scFRAPs presented here was optimized to study the dynamics of Ace2, Fus3, and YFP. The choice of the time resolution and the length of the experiment determine which dynamics can be observed. Given our experimental design, whatever did not change during the experiment, we considered "fixed." However, is possible that these fixed molecules were shuttling on a slower timescale. When applying this method to other proteins, the experimental protocol decisions must be carefully considered for each protein and biological problem.

Our method cannot completely distinguish nuclear from cytoplasmic fixed fractions when both co-exist. For the proteins we studied, we could set an upper boundary for the cytoplasmic fixed fraction that was in all cases less than 20% of the proteins (Data S1 Figure 2). As shown in Data S1 section 3, the presence of a cytoplasmic fixed fraction would not affect the estimated import and export rates, but it could produce a slight over-estimation of the nuclear fixed fraction.

The fact that the population distributions of import/export rates for passive diffusion and the distributions of the number of NPCs proteins have similar variability (Figure 3) is consistent with the notion that variability in NPCs is the source of the variability in the "general machinery" involved in nuclear-cytoplasmic transport. While other sources could also contribute, the observed variation in NPC numbers appears sufficient to explain the variation in import/export rates, and it provides a simple and reasonable explanation. However, this does not prove a causal relationship. Future studies that measure NPC abundance and import/export kinetics in the same cell would be necessary to demonstrate a causal relation between NPCs numbers and nuclear shuttling kinetics.

STAR★METHODS

Detailed methods are provided in the online version of this paper and include the following:

- KEY RESOURCES TABLE
- RESOURCE AVAILABILITY
  - Lead contact
  - Materials availability
  - Data and code availability
- EXPERIMENTAL MODEL AND SUBJECT DETAILS
  - *S. cerevisiae* strains and plasmids
  - Cells preparation for microscopy
- METHOD DETAILS
  - Imaging and scFRAPs assays
  - Data analysis and fitting
- QUANTIFICATION AND STATISTICAL ANALYSIS
  - Statistical testing
  - Estimation of correlated and un-correlated variability
  - Data inclusion/exclusion decision

SUPPLEMENTAL INFORMATION

Supplemental information can be found online at https://doi.org/10.1016/j.isci.2022.105906.

ACKNOWLEDGMENTS

We are grateful to Peter Pryciak and Alejandra Ventura for feedback and advise. We also thank Richard Yu for providing plasmids. We are especially grateful to Linnea Järvstråt, Ulrike Münzner, Karin Wiberg, and Martin Gollvik who participated in different aspects of the modeling and parameter estimation work. Work at GC lab was funded by the Swedish Research Council and at ACL lab by grants PICT2005-33628, PICT2007-847 and PICT2010-2248 from the Argentine Agency of Research and Technology (ANPCyT) to ACL.

AUTHORS CONTRIBUTIONS

LD performed most of the scFRAPs, constructed the strains and some of the plasmids used in the study, and performed modeling and data analysis. AB performed scFRAPs, data analysis, developed the model and

the R package for data fitting. AG performed the measurements of nuclear pore proteins. AK wrote the R package for data fitting. LD, AB, and ACL interpreted the data. RJ supervised DL and MG and performed the analysis with multiple shell models. DL performed the profile likelihood analysis and the implementation with the local optimization algorithm; MG performed the analysis proving that a detailed mechanistic model is equivalent to a two-state model; GC directed the theoretical aspects of the project. LD and ACL conceived the project. LD, AB, and ACL wrote the article.

DECLARATION OF INTERESTS

The authors declare no competing interests.

Received: June 21, 2022
Revised: November 10, 2022
Accepted: December 25, 2022
Published: January 20, 2023

REFERENCES

1. Elowitz, M.B., Levine, A.J., Siggia, E.D., and Swain, P.S. (2002). Stochastic gene expression in a single cell. Science *297*, 1183–1186. https://doi.org/10.1126/science.1070919.

2. Rosenfeld, N., Elowitz, M.B., and Alon, U. (2002). Negative autoregulation speeds the response times of transcription networks. J. Mol. Biol. *323*, 785–793. https://doi.org/10.1016/s0022-2836(02)00994-4.

3. Raser, J.M., and O'Shea, E.K. (2004). Control of stochasticity in eukaryotic gene expression. Science *304*, 1811–1814. https://doi.org/10.1126/science.1098641.

4. Huh, D., and Paulsson, J. (2011). Non-genetic heterogeneity from stochastic partitioning at cell division. Nat. Genet. *43*, 95–100. https://doi.org/10.1038/ng.729.

5. Colman-Lerner, A., Gordon, A., Serra, E., Chin, T., Resnekov, O., Endy, D., Pesce, C.G., and Brent, R. (2005). Regulated cell-to-cell variation in a cell-fate decision system. Nature *437*, 699–706. https://doi.org/10.1038/nature03998.

6. Blake, W.J., KAErn, M., Cantor, C.R., and Collins, J.J. (2003). Noise in eukaryotic gene expression. Nature *422*, 633–637. https://doi.org/10.1038/nature01546.

7. Spencer, S.L., Gaudet, S., Albeck, J.G., Burke, J.M., and Sorger, P.K. (2009). Non-genetic origins of cell-to-cell variability in TRAIL-induced apoptosis. Nature *459*, 428–432. https://doi.org/10.1038/nature08012.

8. Gándara, L., Durrieu, L., Behrensen, C., and Wappner, P. (2019). A genetic toolkit for the analysis of metabolic changes in Drosophila provides new insights into metabolic responses to stress and malignant transformation. Sci. Rep. *9*, 19945. https://doi.org/10.1038/s41598-019-56446-3.

9. Roux, J., Hafner, M., Bandara, S., Sims, J.J., Hudson, H., Chai, D., and Sorger, P.K. (2015). Fractional killing arises from cell-to-cell variability in overcoming a caspase activity threshold. Mol. Syst. Biol. *11*, 803. https://doi.org/10.15252/msb.20145584.

10. Mitchell, S., Vargas, J., and Hoffmann, A. (2016). Signaling via the NFκB system. Wiley Interdiscip. Rev. Syst. Biol. Med. *8*, 227–241. https://doi.org/10.1002/wsbm.1331.

11. St-Pierre, F., and Endy, D. (2008). Determination of cell fate selection during phage lambda infection. Proc. Natl. Acad. Sci. USA *105*, 20705–20710. https://doi.org/10.1073/pnas.0808831105.

12. Vashistha, H., Kohram, M., and Salman, H. (2021). Non-genetic inheritance restraint of cell-to-cell variation. Elife *10*, e64779. https://doi.org/10.7554/elife.64779.

13. Mitchell, S. (2021). What will B will B: identifying molecular determinants of diverse B-cell fate decisions through systems biology. Front. Cell Dev. Biol. *8*, 616592. https://doi.org/10.3389/fcell.2020.616592.

14. Mura, M., Feillet, C., Bertolusso, R., Delaunay, F., and Kimmel, M. (2019). Mathematical modelling reveals unexpected inheritance and variability patterns of cell cycle parameters in mammalian cells. PLoS Comput. Biol. *15*, e1007054. https://doi.org/10.1371/journal.pcbi.1007054.

15. Li, Y., Shan, Y., Desai, R.V., Cox, K.H., Weinberger, L.S., and Takahashi, J.S. (2020). Noise-driven cellular heterogeneity in circadian periodicity. Proc. Natl. Acad. Sci. USA *117*, 10350–10356. https://doi.org/10.1073/pnas.1922388117.

16. Kaufmann, B.B., Yang, Q., Mettetal, J.T., and van Oudenaarden, A. (2007). Heritable stochastic switching revealed by single-cell genealogy. PLoS Biol. *5*, e239. https://doi.org/10.1371/journal.pbio.0050239.

17. Rout, M.P., Aitchison, J.D., Suprapto, A., Hjertaas, K., Zhao, Y., and Chait, B.T. (2000). The yeast nuclear pore complex: composition, architecture, and transport mechanism. J. Cell Biol. *148*, 635–651. https://doi.org/10.1083/jcb.148.4.635.

18. Paine, P.L., and Scherr, P. (1975). Drag coefficients for the movement of rigid spheres through liquid-filled cylindrical pores. Biophys. J. *15*, 1087–1091. https://doi.org/10.1016/s0006-3495(75)85884-x.

19. Yang, W., and Musser, S.M. (2006). Nuclear import time and transport efficiency depend on importin β concentration. J. Cell Biol. *174*, 951–961. https://doi.org/10.1083/jcb.200605053.

20. Mohr, D., Frey, S., Fischer, T., Güttler, T., and Görlich, D. (2009). Characterisation of the passive permeability barrier of nuclear pore complexes. EMBO J. *28*, 2541–2553. https://doi.org/10.1038/emboj.2009.200.

21. Ribbeck, K., and Görlich, D. (2002). The permeability barrier of nuclear pore complexes appears to operate via hydrophobic exclusion. EMBO J. *21*, 2664–2671. https://doi.org/10.1093/emboj/21.11.2664.

22. Nasmyth, K. (1983). Molecular analysis of a cell lineage. Nature *302*, 670–676. https://doi.org/10.1038/302670a0.

23. Sil, A., and Herskowitz, I. (1996). Identification of asymmetrically localized determinant, Ash1p, required for lineage-specific transcription of the yeast HO gene. Cell *84*, 711–722. https://doi.org/10.1016/s0092-8674(00)81049-1.

24. Bobola, N., Jansen, R.P., Shin, T.H., and Nasmyth, K. (1996). Asymmetric accumulation of Ash1p in postanaphase nuclei depends on a myosin and restricts yeast mating-type switching to mother cells. Cell *84*, 699–709. https://doi.org/10.1016/s0092-8674(00)81048-x.

25. Colman-Lerner, A., Chin, T.E., and Brent, R. (2001). Yeast Cbk1 and Mob2 activate daughter-specific genetic programs to induce asymmetric cell fates. Cell *107*, 739–750. https://doi.org/10.1016/s0092-8674(01)00596-7.

26. Jensen, T.H., Neville, M., Rain, J.C., McCarthy, T., Legrain, P., and Rosbash, M. (2000). Identification of novel Saccharomyces cerevisiae proteins with nuclear export activity: cell cycle-regulated transcription factor ace2p shows cell cycle-independent nucleocytoplasmic shuttling. Mol. Cell Biol. *20*, 8047–8058. https://doi.org/10.1128/mcb.20.21.8047-8058.2000.

27. Weiss, E.L., Kurischko, C., Zhang, C., Shokat, K., Drubin, D.G., and Luca, F.C. (2002). The Saccharomyces cerevisiae Mob2p-Cbk1p kinase complex promotes polarized growth and acts with the mitotic exit network to facilitate daughter cell-specific localization of Ace2p transcription factor. J. Cell Biol. *158*, 885–900. https://doi.org/10.1083/jcb.200203094.

28. Mazanka, E., Alexander, J., Yeh, B.J., Charoenpong, P., Lowery, D.M., Yaffe, M., and Weiss, E.L. (2008). The NDR/LATS family kinase Cbk1 directly controls transcriptional asymmetry. PLoS Biol. *6*, e203. https://doi.org/10.1371/journal.pbio.0060203.

29. Boettcher, B., Marquez-Lago, T.T., Bayer, M., Weiss, E.L., and Barral, Y. (2012). Nuclear envelope morphology constrains diffusion and promotes asymmetric protein segregation in closed mitosis. J. Cell Biol. *197*, 921–937. https://doi.org/10.1083/jcb.201112117.

30. Cavalier-Smith, T. (2010). Origin of the cell nucleus, mitosis and sex: roles of intracellular coevolution. Biol. Direct *5*, 7. https://doi.org/10.1186/1745-6150-5-7.

31. O'Conallain, C., Doolin, M.T., Taggart, C., Thornton, F., and Butler, G. (1999). Regulated nuclear localisation of the yeast transcription factor Ace2p controls expression of chitinase (CTS1) in Saccharomyces cerevisiae. Mol. Gen. Genet. *262*, 275–282. https://doi.org/10.1007/s004380051084.

32. Brace, J., Hsu, J., and Weiss, E.L. (2011). Mitotic exit control of the Saccharomyces cerevisiae Ndr/LATS kinase Cbk1 regulates daughter cell separation after cytokinesis. Mol. Cell Biol. *31*, 721–735. https://doi.org/10.1128/mcb.00403-10.

33. Sbia, M., Parnell, E.J., Yu, Y., Olsen, A.E., Kretschmann, K.L., Voth, W.P., and Stillman, D.J. (2008). Regulation of the yeast Ace2 transcription factor during the cell cycle. J. Biol. Chem. *283*, 11135–11145. https://doi.org/10.1074/jbc.M800196200.

34. Bourens, M., Racki, W., Bécam, A.M., Panozzo, C., Boulon, S., Bertrand, E., and Herbert, C.J. (2008). Mutations in a small region of the exportin Crm1p disrupt the daughter cell-specific nuclear localization of the transcription factor Ace2p in Saccharomyces cerevisiae. Biol. Cell *100*, 343–354. https://doi.org/10.1042/BC20070077.

35. Bourens, M., Racki, W., Bécam, A.M., Panozzo, C., Boulon, S., Bertrand, E., and Herbert, C.J. (2008). Mutations in a small region of the exportin Crm1p disrupt the daughter cell-specific nuclear localization of the transcription factor Ace2p in Saccharomyces cerevisiae. Biol. Cell *100*, 343–354. https://doi.org/10.1042/BC20070077.

36. Mazanka, E., and Weiss, E.L. (2010). Sequential counteracting kinases restrict an asymmetric gene expression program to early G1. Mol. Biol. Cell *21*, 2809–2820. https://doi.org/10.1091/mbc.E10-02-0174.

37. Dohrmann, P.R., Butler, G., Tamai, K., Dorland, S., Greene, J.R., Thiele, D.J., and Stillman, D.J. (1992). Parallel pathways of gene regulation: homologous regulators SWI5 and ACE2 differentially control transcription of HO and chitinase. Genes Dev. *6*, 93–104. https://doi.org/10.1101/gad.6.1.93.

38. Herrero, E., Stinus, S., Bellows, E., Berry, L.K., Wood, H., and Thorpe, P.H. (2020). Asymmetric transcription factor partitioning during yeast cell division requires the FACT chromatin remodeler and cell cycle progression. Genetics *216*, 701–716. https://doi.org/10.1534/genetics.120.303439.

39. Boettcher, B., and Barral, Y. (2013). The cell biology of open and closed mitosis. Nucleus *4*, 160–165. https://doi.org/10.4161/nucl.24676.

40. Axelrod, D., Koppel, D.E., Schlessinger, J., Elson, E., and Webb, W.W. (1976). Mobility measurement by analysis of fluorescence photobleaching recovery kinetics. Biophys. J. *16*, 1055–1069. https://doi.org/10.1016/s0006-3495(76)85755-4.

41. Cole, N.B., Smith, C.L., Sciaky, N., Terasaki, M., Edidin, M., and Lippincott-Schwartz, J. (1996). Diffusional mobility of Golgi proteins in membranes of living cells. Science *273*, 797–801. https://doi.org/10.1126/science.273.5276.797.

42. Cole, N.B., Sciaky, N., Marotta, A., Song, J., and Lippincott-Schwartz, J. (1996). Golgi dispersal during microtubule disruption: regeneration of Golgi stacks at peripheral endoplasmic reticulum exit sites. Mol. Biol. Cell *7*, 631–650. https://doi.org/10.1091/mbc.7.4.631.

43. Wachsmuth, M., Weidemann, T., Müller, G., Hoffmann-Rohrer, U.W., Knoch, T.A., Waldeck, W., and Langowski, J. (2003). Analyzing intracellular binding and diffusion with continuous fluorescence photobleaching. Biophys. J. *84*, 3353–3363. https://doi.org/10.1016/s0006-3495(03)70059-9.

44. Goodwin, J.S., and Kenworthy, A.K. (2005). Photobleaching approaches to investigate diffusional mobility and trafficking of Ras in living cells. Methods *37*, 154–164. https://doi.org/10.1016/j.ymeth.2005.05.013 PMID - 16288889.

45. Gordon, A., Colman-Lerner, A., Chin, T.E., Benjamin, K.R., Yu, R.C., and Brent, R. (2007). Single-cell quantification of molecules and rates using open-source microscope-based cytometry. Nat. Methods *4*, 175–181. https://doi.org/10.1038/nmeth1008.

46. Lippincott, J., and Li, R. (1998). Sequential assembly of myosin II, an IQGAP-like protein, and filamentous actin to a ring structure involved in budding yeast cytokinesis. J. Cell Biol. *140*, 355–366. https://doi.org/10.1083/jcb.140.2.355.

47. Dohlman, H.G., and Thorner, J.W. (2001). Regulation of G protein-initiated signal transduction in yeast: paradigms and Principles. Annu. Rev. Biochem. *70*, 703–754. https://doi.org/10.1146/annurev.biochem.70.1.703.

48. van Drogen, F., Stucke, V.M., Jorritsma, G., and Peter, M. (2001). MAP kinase dynamics in response to pheromones in budding yeast. Nat. Cell Biol. *3*, 1051–1059. https://doi.org/10.1038/ncb1201-1051.

49. Racki, W.J., Bécam, A.M., Nasr, F., and Herbert, C.J. (2000). Cbk1p, a protein similar to the human myotonic dystrophy kinase, is essential for normal morphogenesis in saccharomyces cerevisiae. EMBO J. *19*, 4524–4532. https://doi.org/10.1093/emboj/19.17.4524.

50. Jensen, T.H., Neville, M., Legrain, P., and Rosbash, M. (2000). Identification of novel Saccharomyces cerevisiae proteins with nuclear export activity: cell cycle-regulated transcription factor Ace2p shows cell cycle-independent nucleocytoplasmic shuttling TORBEN. Society *20*, 8047–8058.

51. Fu, A.Q., and Pachter, L. (2016). Estimating intrinsic and extrinsic noise from single-cell gene expression measurements. Stat. Appl. Genet. Mol. Biol. *15*, 447–471. https://doi.org/10.1515/sagmb-2016-0002.

52. Khmelinskii, A., Keller, P.J., Lorenz, H., Schiebel, E., and Knop, M. (2010). Segregation of yeast nuclear pores. Nature *466*, E1. https://doi.org/10.1038/nature09255.

53. Huh, W.K., Falvo, J.V., Gerke, L.C., Carroll, A.S., Howson, R.W., Weissman, J.S., and O'Shea, E.K. (2003). Global analysis of protein localization in budding yeast. Nature *425*, 686–691. https://doi.org/10.1038/nature02026.

54. Lewontin, R.C. (1966). On the measure of relative variability. Syst. Zool. *15*, 141–142. https://doi.org/10.2307/2411632.

55. Winey, M., Yarar, D., Giddings, T.H., and Mastronarde, D.N. (1997). Nuclear pore complex number and distribution throughout the Saccharomyces cerevisiae cell cycle by three-dimensional reconstruction from electron micrographs of nuclear envelopes. Mol. Biol. Cell *8*, 2119–2132. https://doi.org/10.1091/mbc.8.11.2119.

56. Siebrasse, J.P., and Peters, R. (2002). Rapid translocation of NTF2 through the nuclear pore of isolated nuclei and nuclear envelopes. EMBO Rep. *3*, 887–892. https://doi.org/10.1093/embo-reports/kvf171.

57. Timney, B.L., Tetenbaum-Novatt, J., Agate, D.S., Williams, R., Zhang, W., Chait, B.T., and Rout, M.P. (2006). Simple kinetic relationships and nonspecific competition govern nuclear import rates in vivo. J. Cell Biol. *175*, 579–593. https://doi.org/10.1083/jcb.200608141.

58. Nemergut, M.E., and Macara, I.G. (2000). Nuclear import of the ran exchange factor, Rcc1, is mediated by at least two distinct mechanisms. J. Cell Biol. *149*, 835–850. https://doi.org/10.1083/jcb.149.4.835.

59. Ribbeck, K., Görlich, D., and Go, D. (2001). Kinetic analysis of translocation through

nuclear pore complexes. EMBO J. *20*, 1320–1330.

60. Kiskin, N.I., Siebrasse, J.P., and Peters, R. (2003). Optical microwell assay of membrane transport kinetics. Biophys. J. *85*, 2311–2322. https://doi.org/10.1016/S0006-3495(03)74655-4.

61. Frey, S., Rees, R., Schünemann, J., Ng, S.C., Fünfgeld, K., Huyton, T., and Görlich, D. (2018). Surface properties determining passage rates of proteins through nuclear pores. Cell *174*, 202–217.e9. https://doi.org/10.1016/j.cell.2018.05.045.

62. Ribbeck, K., and Görlich, D. (2001). Kinetic analysis of translocation through nuclear pore complexes. EMBO J. *20*, 1320–1330. https://doi.org/10.1093/emboj/20.6.1320.

63. Jorgensen, P., Edgington, N.P., Schneider, B.L., Rupes, I., Tyers, M., and Futcher, B. (2007). The size of the nucleus increases as yeast cells grow. Mol. Biol. Cell *18*, 3523–3532. https://doi.org/10.1091/mbc.E06.

64. Uchida, M., Sun, Y., McDermott, G., Knoechel, C., Le Gros, M.A., Parkinson, D., Drubin, D.G., and Larabell, C.A. (2011). Quantitative analysis of yeast internal architecture using soft X-ray tomography. Yeast *28*, 227–236. https://doi.org/10.1002/yea.1834.

65. Webster, M.T., McCaffery, J.M., and Cohen-Fix, O. (2010). Vesicle trafficking maintains nuclear shape in Saccharomyces cerevisiae during membrane proliferation. J. Cell Biol. *191*, 1079–1088. https://doi.org/10.1083/jcb.201006083.

66. Vashistha, H., Kohram, M., and Salman, H. (2021). Non-genetic inheritance restraint of cell-to-cell variation. Elife *10*, e64779. https://doi.org/10.7554/eLife.64779.

67. Sigal, A., Milo, R., Cohen, A., Geva-Zatorsky, N., Klein, Y., Liron, Y., Rosenfeld, N., Danon, T., Perzov, N., and Alon, U. (2006). Variability and memory of protein levels in human cells. Nature *444*, 643–646.

68. Süel, G.M., Garcia-Ojalvo, J., Liberman, L.M., and Elowitz, M.B. (2006). An excitable gene regulatory circuit induces transient cellular differentiation. Nature *440*, 545–550. https://doi.org/10.1038/nature04588.

69. Neville, M., and Rosbash, M. (1999). The NES-Crm1p export pathway is not a major mRNA export route in Saccharomyces cerevisiae. EMBO J. *18*, 3746–3756. https://doi.org/10.1093/emboj/18.13.3746.

70. Bush, A., Chernomoretz, A., Yu, R., Gordon, A., and Colman-Lerner, A. (2012). Using Cell-ID 1.4 with R for microscope-based cytometry. Curr. Protoc. Mol. Biol. *14*. https://doi.org/10.1002/0471142727.mb1418s100.

71. Team, R.D.C. (2010). R: A Language and Environment for Statistical Computing.

72. Rasband, W.S. (1997-2005) (ImageJ. N.I.H.). http://rsb.info.nih.gov/ij/.

73. Ausubel, F.M., Brent, R., Kingston, R.E., Moore, D.D., Seidman, J.G., Smith, J.A., and Struhl, K. (1987-2017). Current Protocols in Molecular Biology (John Wiley & Sons, Inc.).

74. Silverman, S. (1991). Methods in enzymology vol. 194, guide to yeast genetics and molecular biology. Edited by Christine Guthrie and Gerald R. Fink. Academic Press, San Diego, CA, 1990. 933 pp. Anal. Biochem. *196*, 199–200. https://doi.org/10.1016/0003-2697(91)90140-O.

75. Fu, A.Q., and Pachter, L. (2016). Estimating intrinsic and extrinsic noise from single-cell gene expression measurements. Stat. Appl. Genet. Mol. Biol. *15*, 447–471. https://doi.org/10.1515/sagmb-2016-0002.

STAR★METHODS

KEY RESOURCES TABLE

REAGENT or RESOURCE	SOURCE	IDENTIFIER
Critical commercial assays		
384-well glass bottom plates	Matrical Biosciences	MGB101-1-1-LG
Deposited data		
Raw data from the quantification of the FRAP experiments	This paper	https://doi.org/10.17632/wfhgv3hxn6.1
Experimental models: Organisms/strains		
S. cerevisiae: Strain background: W303 Relevant genotype: ura3::PAct1-YFP stop, bar1Δ ID: TCY-3081	Colman-Lerner et al., 2001[25]	N/A
S. cerevisiae: Strain background: S288C Relevant genotype: MYOI::MYO1-CHERRY: Mx6-Hyg ID: LDY-3470	This paper	N/A
S. cerevisiae: Strain background: S288C Relevant genotype: NUP49-GFP	Huh et al., 2003[53]	N/A
S. cerevisiae: Strain background: S288C Relevant genotype: MPL1-GFP	Huh et al., 2003[53]	N/A
S. cerevisiae: Strain background: S288C Relevant genotype: MPL2-GFP	Huh et al., 2003[53]	N/A
S. cerevisiae: Strain background: S288C Relevant genotype: CRM1-T539C	Neville et al., 1999[69]	N/A
Oligonucleotides		
Primer: tagging of Myo with mCherry Forward: AAATATTGATAGTAACAATGCACAGAGTAAA ATTTTCAGTATGGCAACTAGCGGCATGGTT	This paper	N/A
Primer: tagging of Myo with mCherry Reverse: GTTAATAATGCATATTCTCATTCTGTATATACAA AACATCATAGGCCACTAGTGGATCTG	This paper	N/A
Recombinant DNA		
Plasmid: YFP-Ace2	Colman-Lerner et al., 2001[25]	N/A
Plasmid: CFP-Ace2	Colman-Lerner et al., 2001[25]	N/A
Plasmid: YFP-Ace2 G128E	Colman-Lerner et al., 2001[25]	N/A
Plasmid: Fus3-Ace2		N/A
Plasmid: Pry2060 (mCherry, Hyg)	Gift from Richard Yu	N/A
Software and algorithms		
NuclearFRAP. R package for model fitting of trains of FRAPs data, from mother-daughter pairs of cells	This paper	https://doi.org/10.17632/wfhgv3hxn6.1
Rcell. R package for cell cytometry.	Bush et al. 2012[70]	http://sourceforge.net/projects/cell-id
R	R Development Team (2010)[71]	http://www.r-project.org/
ImageJ	Rasband, 1997–2005[72]	https://imagej.nih.gov/ij/
Time series analyzer (RRID:SCR_014269). ImageJ plugin	Balaji J. Dept. of Neurobiology, UCLA	https://imagej.nih.gov/ij/plugins/time-series.html

RESOURCE AVAILABILITY

Lead contact

Further information and requests for resources and reagents should be directed to and will be fulfilled by the lead contact, Alejandro Colman-Lerner (colman-lerner@fbmc.fcen.uba.ar).

Materials availability

Plasmids and yeast strains generated in this study are available upon request.

Data and code availability

- The datasets resulting from the quantification of the FRAP experiments study are publicly available, and can be found at Mendeley Data: https://doi.org/10.17632/wfhgv3hxn6.1 as of the date of publication. Raw microscopy images reported in this paper will be shared by the lead contact upon request.
- The NuclearFRAP R package, has been deposited at Mendelay Data and is publicly available as of the date of publication, Mendeley Data: https://doi.org/10.17632/wfhgv3hxn6.1.
- Any additional information required to reanalyze the data reported in this paper is available from the lead contact upon request.

EXPERIMENTAL MODEL AND SUBJECT DETAILS

S. cerevisiae strains and plasmids

We performed general molecular biology procedures, yeast strain manipulation and construction according to previously established methods.[73,74]

All strains generated and used in this study are listed in the key resources table.

Tagging of Myo1 with mCherry was performed by homologous recombination by transforming the appropriate strains with a PCR fragment containing mCherry followed by a hygromycin resistance cassette, flanked by 40 nucleotides of homology with the end of the MYO1 ORF (except the STOP codon) on its 5′ end and the region of the 3′ UTR from +50 to +90. We used as template for this PCR plasmid Pry2 2060.1 Hyg. The sequence of the primers is listed in the the key resources table.

We selected transformants in plates with YPD plates with hygromycin and confirmed that integration occurred in the right location by visual determination of the presence of the red fluorescent ring at the bud-neck.

All plasmids generated and used in this study are listed in the key resources table.

Cells preparation for microscopy

Yeast cells were prepared for the scFRAPs experiments by growing them at least two consecutive days on selective BSM-TRP LEU URA 2% glucose plates. Then yeast from the least grown part of a streak were picked, resuspended in BSM-TRP, LEU, URA 2% glucose liquid media and added to a 384-well glass bottom plates (MGB101-1-1-LG, Matrical Biosciences). To prevent cells from moving, we pre-treated the wells with concanavalin A (type V; Sigma-Aldrich, St. Louis, MO). To do this, we added to each well 50 µl of a 100 mg/mL solution of concanavalin A in water, incubated at least for 20 min at room temperature (18–23 1C), and then washed 2 times with water. Cells were allowed to settle on the plate for 10–20 min and then we removed the supernatant and added 50 µL of fresh selective medium.

METHOD DETAILS

Imaging and scFRAPs assays

The scFRAPs were performed in an Olimpus IX-81 inverted microscope with an FV1000 confocal module with an oil immersion Olympus UplanSapo 63× objective (numerical aperture, NA 1.35). For the experiments we used an automatic z axis control, a motorized x-y stage, a 458-488-515 argon and a 543 He-Ne lasers, and Hamamatsu R6353 photomultipliers (PMTs).

Cells in the desired stage of the cell cycle were identified, then reference images of the transmission, CFP and mCherry channels (to observe Ace2-CFP and Myo1-mCherry) were acquired. Then 4 consecutive FRAPs were performed in the YFP channel. Each FRAP consisted of 5 initial images, followed by a partial photobleaching of the nucleus, and 30 images to follow the recovery. The time resolution was 0.2 s.

Data analysis and fitting

For a detailed description of the protocols for image acquisition, data correction and fitting, see Data S1, section 4. Briefly, the images were quantified with the ImageJ plugin Time Series Analyzer. Then, model fitting was performed with our own R package, NuclearFRAP.

QUANTIFICATION AND STATISTICAL ANALYSIS

Statistical testing

The number of data points -individual cells or mother-daughter pairs of cells depending on the case-for each analysis can be found in the figure legend.

All estimated parameters are presented as median ±SEM When indicated, statistical significance was calculated using Student's two-sample t-test (unpaired two samples for means) over the logarithms of the values (with base 10). P-values are informed only for significant ($p < 0.05$) differences.

Comparisons between variances were performed according to Lewontin (1966).[54] The variance of the logarithms of the values (with base 10) was contrasted by an F-test. P-values are informed only for significant ($p < 0.05$) differences. This analysis permits comparison of relative variances for values with different means, without requiring normality.

The error bars for the correlation and SD in Figure 3 were produced by bootstrapping 1000 times with reposition samples of 90% the size of the data for the experiment, estimating either the correlation or the SD according to the case, and then defining the interval that contained 95% of the estimated values.

Estimation of correlated and un-correlated variability

For the analysis in Figure 3, where the cell-to-cell variability in transport rates was decomposed into correlated and un-correlated, the following estimators were used (after Qiuyan Fua et al. (2016)[75]).

$$Correlated\ variation = \frac{1}{n-1} * \frac{\sum_{i=1}^{n} K_{Ii} * K_{Ei} - n * <K_I> * <K_E>}{<K_I> * <K_E>}$$

$$Un-correlated\ variation = \frac{1}{2*(n-1)} * \frac{\sum_{1}^{n} (K_{Ii} - K_{Ei})^2 - n * (<K_I> - <K_E>)^2}{<K_I> * <K_E>}$$

Data inclusion/exclusion decision

Prior to analysis and fitting, the acquired images were manually curated in order to discard experiments that had technical issues, such as cells movement or focus drift. After fitting, data for which no statistically acceptable parameters were found was filtered out. This represented approximately 15% of the single-cells data, and was due in general to the optimal parameters laying outside of the pre-defined region of the parameter space that our experimental protocol could reliably assay. No data points were excluded during the biological analysis.